SCIENCE CHINA
Technological Sciences

•Article•

July 2019 Vol.62 No.7: 1067–1081
https://doi.org/10.1007/s11431-018-9404-9

Jerk-limited feedrate scheduling and optimization for five-axis machining using new piecewise linear programming approach

SUN YuWen[1*], CHEN ManSen[1], JIA JinJie[1], LEE Yuan-Shin[2] & GUO DongMing[1]

[1] *School of Mechanical Engineering, Dalian University of Technology, Dalian 116024, China;*
[2] *Department of Industrial and Systems Engineering, North Carolina State University, Raleigh NC 27695, USA*

Received September 30, 2018; accepted December 3, 2018; published online June 5, 2019

In this paper, a new computation method and an optimization algorithm are presented for feedrate scheduling of five-axis machining in compliance with both machine drive limits and process limits. Five-axis machine tool with its ability of controlling tool orientation to follow the sculptured surface contour has been widely used in modern manufacturing industry. Feedrate scheduling serving as a kernel of CNC control system plays a critical role to ensure the required machining accuracy and reliability for five-axis machining. Due to the nonlinear coupling effects of all involved drive axes and the saturation limit of servo motors, the feedrate scheduling for multi-axis machining has long been recognized and remains as a critical challenge for achieving five-axis machine tools' full capacity and advantage. To solve the nonlinearity nature of the five-axis feedrate scheduling problems, a relaxation mathematical process is presented for relaxing both the drive motors' physical limitations and the kinematic constraints of five-axis tool motions. Based on the primary optimization variable of feedrate, the presented method analytically linearizes the machining-related constraints, in terms of the machines' axis velocities, axis accelerations and axis jerks. The nonlinear multi-constrained feedrate scheduling problem is transformed into a manageable linear programming problem. An optimization algorithm is presented to find the optimal feedrate scheduling solution for the five-axis machining problems. Both computer implementation and laboratorial experiment testing by actual machine cutting were conducted and presented in this paper. The experiment results demonstrate that the proposed method can effectively generate efficient feedrate scheduling for five-axis machining with constraints of the machine tool physical constraints and limits. Compared with other existing numerical methods, the proposed method is able to find an accurate analytical solution for the nonlinear constrained five-axis feedrate scheduling problems without compromising the efficiency of the machining processes.

five-axis machining, feedrate scheduling, jerk, linear programming, optimization

Citation: Sun Y W, Chen M S, Jia J J, et al. Jerk-limited feedrate scheduling and optimization for five-axis machining using new piecewise linear programming approach. Sci China Tech Sci, 2019, 62: 1067–1081, https://doi.org/10.1007/s11431-018-9404-9

1 Introduction

With the growing demand for high performance sculptured surface parts in the field of aerospace, automobile, consumer products, die and mold manufacturing, five-axis machine tools have been widely used in modern manufacturing industry. Five-axis machine tools provide excellent ability to achieve excellent machined surface quality, and better tool motion flexibility for complex parts machining that cannot possibly be machined on a traditional 3-axis machine tool. In the last decade, many researchers had focused their research on the parametric interpolation [1,2], kinematics and geometrical error modeling [3–5], efficient tool-path generation [6,7], real time contour error estimation [8,9] and constrained feedrate scheduling [10,11]. Among them, the feedrate scheduling, which serves as a kernel factor that determines the machining productivity and dimensional accuracy, is recently gaining significant attention from the NC manu-

*Corresponding author (email: xiands@dlut.edu.cn)

© Science China Press and Springer-Verlag GmbH Germany, part of Springer Nature 2019

facturers industry and research community. To achieve the maximum productivity, the tool axis traverse rates and spindle speeds are typically required to be as large as possible [12]. Due to the nonlinearity and complex nature of the five-axis feedrate scheduling problem, in reality, engineers typically select a conservative feedrate on machine tools to avoid errors that compromise the machined surface quality or to prevent any possible unflavored mechanical jerks during complex tool motion. This will result in a sacrifice of the efficiency of five-axis machine tools and a prolonged machining time, both are unfavorable for manufacturing practice. Therefore, how to plan an optimal feedrate profile with improved kinematical property and the minimum total machining time remains a very important and critical problem to be solved for realizing the high performance of five-axis machine tools.

To improve the stability of machining process, techniques of toolpath smoothing for soft feed motion were developed earlier in refs. [13–17]. Yuen et al. [16] proposed a unified spline interpolation method for five-axis machining, where the tool tip and orientation locations are modeled as quantic splines independently to maintain geometric C^3 continuity. Huang et al. [17] gave an analytical local corner smoothing algorithm for five-axis CNC machining by eliminating the corners of tool-path and sudden change of tool orientations with cubic B-splines. Excessive acceleration changes may still possibly occur along the path with sharp curvature changes, causing unstable vibration to cutter axis and result in poor surface finish. For a satisfactory tool motion performance and machining accuracy, different feedrate interpolation methods were developed earlier with the considerations of the acceleration constraints [18], the cutting mechanics [19,20] or the minimal feedrate fluctuation [21]. For example, Yong and Narayanaswami [18] proposed an adaptive feedrate interpolation algorithm with the constraints of chord error and acceleration for machining of parameter curves. Erdim et al. [19] presented a cutting force based feedrate scheduling method for 3-axis milling. Erkorkmaz and Altintas [21] introduced a feed correction polynomial concept and proposed an accurate interpolation method for quintic spline to minimize the feedrate fluctuation.

Another challenge in multi-axis machining is to minimize the residual vibration introduced by high frequency jerks. Several techniques, like the classical look-ahead algorithm [22,23], sine-curve [24] and s-shape curve [25,26], have been developed to generate a jerk-limited feed profile. However, these methods suffer from lacking of sufficient consideration of the "hard limits" of machine tool driving servo actuators' physical capability, typically due to an over-simplification of the assumptions in the earlier study efforts. This could lead into early tool wear or even possible damage to the mechanical structure of the machine tools.

To handle this issue, dichotomy iteration algorithm [27], bidirectional scanning algorithm [28] and curve evolution algorithm [29] have been presented to solve the problems of feedrate interpolation with confined axis jerk constraints. However, solving such constrained nonlinear problem is generally computation intensive and time-consuming. Different methods, like the sequential quadratic programming (SQP) algorithm [30] and the greedy algorithm [31], have been used to realize the optimality. On the other hand, if problems could be possibly formulated as linear problems, finding optimal solution is more feasible and easier to be realized [32–36]. For example, by approximating the nonlinear jerk constraint with its upper bounds, i.e., "pseudo-jerk", Fan et al. [32] first developed a linear programming based time-optimal feedrate scheduling algorithm for five-axis machining, and the square of feedrate (namely f^2) is determined as the optimization variable . Utilizing the same approximation strategy, Guo et al. [33] converted the jerk-limited feedrate optimization into a finite-state convex optimization problem, and proved that the tracking error constraints can be also reduced to a kinematic constraint, thus allowing an accurate path tracing with constraints being fulfilled. Afterwards, some other extended investigations with the linear programming algorithm were presented by Liu et al. [34], and Erkorkmaz et al. [35]. In our earlier works presented in ref. [36], a multi-constrained feedrate scheduling method for the parametric interpolation has been presented. The kinematical characters of cutter tip and drive axes, as well as the angular acceleration of cutter axis, are simultaneously considered and reconfigurable to the requirements of users. However, due to the nature of the complex five-axis machining with multiple constraints, strong nonlinearity exists between the jerk constraints and the primary variable **f**. None of these prior works has attempted to derive the analytical solution of the primary feedrate **f**. For solving such complex problems, numerical approximation methods are typically used at the expense of deteriorating control accuracy of constraints and finding feasible possible solutions, in which extra curve-fitting on the optimal discrete feedrate values are needed for generating the final executable feed profile.

In this paper, a new method of jerk-limited feedrate interpolation and optimization is presented for five-axis machining satisfying both the servo drive physical limits and the tool motion constraints. The remainder of this paper is organized as follows: Sect. 2 presents the feedrate optimization model subject to the kinematic constraints of drive axes and cutter. Sect. 3 shows the related linear representations of the constraints to be considered. The developed piecewise linear programming algorithm and the detailed implementations are shown in Sect. 4. Lab experiments and results are discussed in Sect. 5, and Sect. 6 provides the concluding remarks.

2 Feed optimization model for five-axis machining

Figure 1 shows the digital chain of the CNC control system to be considered, and the proposed feedrate scheduling technique, which actually serves as an interface between the CAM system and NC system, is primarily focused on the process optimization stage. Different from the previous works, the explicit analytical solutions for the multi-constrained feedrate scheduling with respect to the primary feedrate (**f**) are first to be developed. On this basis, a new piecewise linear programming scheme is introduced in detail, which has a new capability to handle the complex machine tool motion and to ensure the C^2 continuity between adjacent feed profiles.

In practice, a dedicated post processor is typically used for five-axis machine tool to transform the cutter locations [**p**(u),**o**(u)] defined in the workpiece coordinate system (WCS) into the corresponding axis drive displacements $\mathbf{m}(u)=[x(u),y(u),z(u),\theta_a(u),\theta_c(u)]^{\mathrm{T}}$ in the machine coordinate system (MCS), as shown in Figure 2. In this paper, five-axis tool paths are generated as the dual NURBS curves for better path description and path smoothness. Without losing generality, assuming both the cutter tip location **p**(u) and the tool orientation **o**(u) in WCS are parameterized with the normalized arc-length parameter u, accordingly, the tool axis drive displacement **m**(u) is defined as a function of arc-length parameter u. The issue of time-optimal feedrate scheduling is then formulated as a constrained optimization problem. Details of such formulations are discussed in the following sections.

2.1 Servo drives and process constraints

Given a reference five-axis toolpath [**p**(u),**o**(u)] in WCS and its corresponding tool axis drive displacement **m**(u) in MCS, then the dynamic performances of each drive axis can be analytically formulated as follows:

$$V^{\tau}=\mathrm{d}m^{\tau}(u)/\mathrm{d}t, A^{\tau}=\mathrm{d}V^{\tau}/\mathrm{d}t, J^{\tau}=\mathrm{d}A^{\tau}/\mathrm{d}t, \tag{1}$$

where V^{τ}, A^{τ}, $J^{\tau}(\tau=x,y,z,\theta_a,\theta_c)$ are the velocity, acceleration and jerk of each drive axis, respectively.

As stated earlier, since the path parameter u is defined as the normalized arc-length parameter, the path parameter u can be derived easily as a linear relation with the arc length s, namely $s=\sigma u$, where σ indicates the total length of the cutter tip curve **p**(u) and $u\in[0,1]$. Thus, let m_u^{τ}, m_{uu}^{τ} and m_{uuu}^{τ} stand for the first, second and third order derivatives of axis drive displacement with respect to the parameter u of cutter tip path curve, and $\dot{f}$, $\ddot{f}$ represent the time derivatives of feedrate, namely the tangential feed acceleration and tangential feed jerk. Then for an arbitrary parameter position u along the path curve **p**(u), the velocity V, the acceleration A and jerk J of a machine tool drive axis can be calculated as

$$\begin{cases} V^{\tau}=m_u^{\tau}f/\sigma, \\ A^{\tau}=(m_{uu}^{\tau}f^2+m_u^{\tau}\sigma\dot{f})/\sigma^2, \\ J^{\tau}=(m_{uuu}^{\tau}f^3+3m_{uu}^{\tau}\sigma\dot{f}f+m_u^{\tau}\sigma^2\ddot{f})/\sigma^3, \end{cases} \tag{2}$$

where

$$\begin{cases} \dot{f}=\mathrm{d}f(u)/\mathrm{d}t=f_u f/\sigma, \\ \ddot{f}=\mathrm{d}\dot{f}/\mathrm{d}t=(f_{uu}f^2+f_u^2 f)/\sigma^2. \end{cases} \tag{3}$$

In eq. (3), f_u and f_{uu} respectively represent the first and the second order derivatives of the feed rate $f(u)$ with respect to the path parameter u.

To guarantee a stable cutting process without violating the physical capacity limits of actuators, the drive constraints for the feedrate scheduling can be formulated as follows:

$$|V^{\tau}|<V_{\max}^{\tau};\ |A^{\tau}|<A_{\max}^{\tau};\ |J^{\tau}|<J_{\max}^{\tau}, \tag{4}$$

where $V_{\max}^{\tau}$, $A_{\max}^{\tau}$ and $J_{\max}^{\tau}$ represent the maximum allowable limits of the velocity, the acceleration and the jerk of each machine tool axis drive.

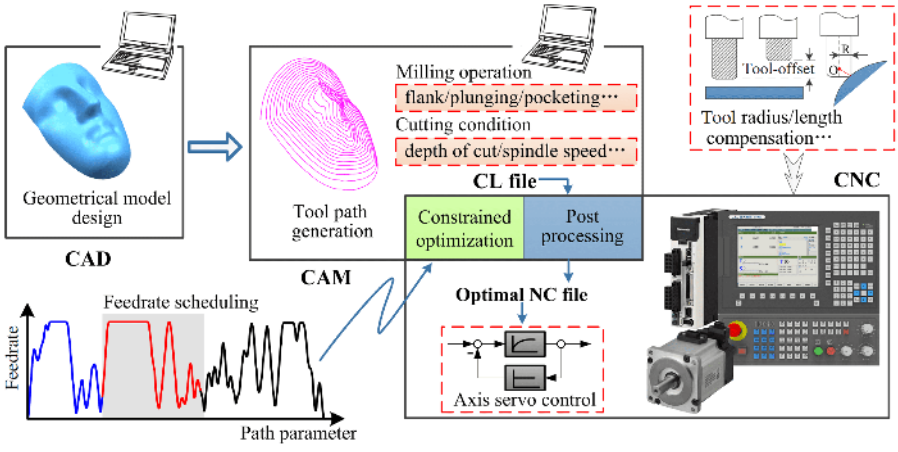

Figure 1 (Color online) Digital chain of multi-axis computer numerical control system.

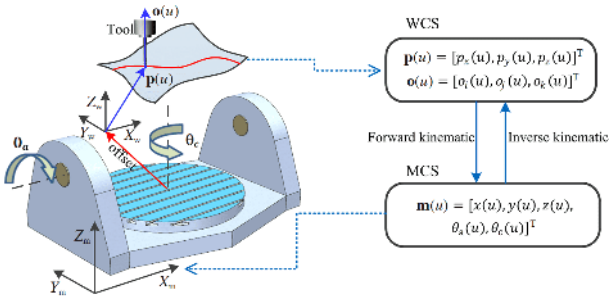

Figure 2 (Color online) Kinematics configuration of the tilting-rotary-table type five-axis machine tool.

Besides the drive constraints for the feedrate scheduling, it is also important to satisfy the kinematic restrictions of cutter movement, since excess feed fluctuations induced by the dramatic change in cutter movement may possibly lead to the deterioration of the machined surface quality. By considering the kinematic limits of cutter tip motion, one has the following additional inequality conditions:

$$f < f_{\max}; |\dot{f}| < A_{c,\max}; |\ddot{f}| < J_{c,\max}, \tag{5}$$

where $f_{\max}$ is the maximum feedrate limit; $A_{c,\max}$ and $J_{c,\max}$ are respectively the maximum tangential acceleration limit and the maximum tangential jerk limit, which can be determined by the process requirements. Thus, taking into account both the physical limits of machine drives and the process limits of the cutter, the feedrate optimization problems along a given toolpath can be formulated. Details are presented in the next section.

2.2 Feedrate optimization modeling

Feedrate optimization problem for a multi-axis CNC control system is to identify a maximum feasible feedrate profile along a predefined toolpath so that the cutting process is executed with the minimum total machining time while simultaneously satisfying the prescribed constraints and limits imposed by the requirement of process planner or the load capacity of the machine tool itself. Taking the formulation of constraints discussed in Sect. 2.1, the time-optimal feedrate scheduling problem can be formulated as follows:

$$\max_f \int_0^1 f(u)\mathrm{d}u,$$

subject to:

$$\begin{cases} f < f_{\max}, |\dot{f}| < A_{c,\max}, |\ddot{f}| < J_{c,\max}, \\ |V^\tau| < V^\tau_{\max}, |A^\tau| < A^\tau_{\max}, |J^\tau| < J^\tau_{\max}. \end{cases} \tag{6}$$

From eqs. (2) and (3), it can be seen that both the machining process constraints $(\dot{f}, \ddot{f})$ and the machine dynamic performance (V^τ, A^τ, J^τ) of the machine feed drives are highly nonlinear functions with the primary variable of feedrate **f**. To solve such nonlinear problems, a typical solution approach is to search for feasible solutions by iterations and time-consuming searching algorithms, as mentioned earlier in the literature review. For five-axis machining with the complex tool motion and the need of real-time control challenge, it is of great interest to find a better solution approach to solve such nonlinear feedrate scheduling problems. In this paper, we propose a mathematical processing technique to efficiently find the feasible and optimal solution of feedrate scheduling problems in a linearly effective way. Details of the proposed method are discussed in the next section.

3 Constraints linearization with respect to feedrate

To solve the nonlinear problems of feedrate scheduling, a method of decoupling nonlinear acceleration and jerk constraints is presented in this section. To solve the feedrate optimization problem, an algorithm of finding an optimal solution for five-axis machining feedrate scheduling is also presented in a later section.

To find the required feedrate profile for the feedrate scheduling, the first task is to decouple the nonlinear acceleration and jerk constraints from the primary feedrate f as well as its associated derivatives (f_u, f_{uu}). After the decoupling of the constraints, a mathematic processing technique is developed to establish a linear relationship between the constraints and feedrate. For constraints linearization, the nonlinear constraints are reformulated to linear ones with an explicit expression of feedrate **f**. By doing so, the aforementioned feedrate scheduling problem is then reduced to find the optimal solution with linear constraints. To achieve this goal, some existing parametric curve patterns, such as polynomial parameter curve and Bezier curve, can all be used to model the feedrate profile. Considering NURBS curve has been widely used in the representation of curve and surface, without loss of generality, a cubic B-spline curve is used here to define the feedrate profile $f(u)$ as a function of path parameter u with the following expression:

$$f(u) = \sum_{i=0}^{Q-1} N_{i,k}(u) D_i, \ u \in [0,1], \tag{7}$$

where $\{D_i\}_0^{Q-1}$ are the control points of the predefined B-spline feedrate profile, Q represents the number of control points, $N_{i,k}(u)$ is the B-spline basis function, k is the degree of the B-spline, and $[u_0, ..., u_{Q+k}]$ represents the knot vector sequence. Differentiating eq. (7) with respect to the path parameter u, then eq. (7) becomes

$$\begin{cases} f_u(u) = \sum_{i=0}^{Q-1} N'_{i,k}(u) D_i, \\ f_{uu}(u) = \sum_{i=0}^{Q-1} N''_{i,k}(u) D_i. \end{cases} \tag{8}$$

From eqs. (7) and (8), it reveals that $f(u)$, $f_u(u)$ and $f_{uu}(u)$ are linearly represented by the vector of control points $\{D_i\}_0^{Q-1}$. Thus, the control points $\{D_i\}_0^{Q-1}$ essentially become the decision variables for the feedrate optimization. In other words, the constrains linearization with respect to the feedrate profile $f(u)$ also means to identify a linear relation between the constraints and the control points $\{D_i\}_0^{Q-1}$. Consequently it becomes the basis in the constraints linearization, as discussed in the following sections.

3.1 Axis acceleration linearization

Given a predefined tool-path and feedrate profile $f(u)$, by combining eqs. (2)–(4), the inequality of acceleration term in eq. (4) can be described as follows:

$$\left| \frac{1}{\sigma^2} (m_{uu}^{\tau} f^2 + m_u^{\tau} f_u f) \right| < A_{\max}^{\tau}. \tag{9}$$

Assuming there exists an approximate feedrate upper limit f^* and $(f < f^*)$ that fulfills all of the constraints mentioned above, then, by using a scale down operation, eq. (9) can be easily rearranged to the following:

$$-\sigma^2 \frac{A_{\max}^{\tau}}{f^*} < m_{uu}^{\tau} f + m_u^{\tau} f_u < \sigma^2 \frac{A_{\max}^{\tau}}{f^*}. \tag{10}$$

This relaxation technique of condition has been proved in earlier cases [32]. It was shown that if the specified feedrate upper limit f^* is close enough to the final optimal one, the loss of optimality would be minimal.

3.2 Axis jerk linearization

From eqs. (2) and (3), it is noticed that the axis jerk constraint is highly coupled with the functions of f, f_u and f_{uu}. In this situation, it is difficult to realize the linearization of axis jerk. To handle the issue, the expression of axis jerk constraint in eq. (2) is rearranged by integrating the axis acceleration term, shown as follows:

$$J^{\tau} = \frac{1}{\sigma^3} \left(m_{uuu}^{\tau} f^3 + 2 m_{uu}^{\tau} f^2 f_u + m_u^{\tau} f_{uu} f^2 \right) + \frac{1}{\sigma} A^{\tau} f_u. \tag{11}$$

Then, using the same relaxation operation of the acceleration as in eqs. (9) and (10), the inequality of the axis jerk term in eq. (4) can be formulated as follows:

$$\left| \frac{f^2}{\sigma^3 (f^*)^2} (m_{uuu}^{\tau} f + 2 m_{uu}^{\tau} f_u + m_u^{\tau} f_{uu}) + \frac{1}{\sigma (f^*)^2} A^{\tau} f_u \right| < \frac{J_{\max}^{\tau}}{(f^*)^2}. \tag{12}$$

Considering the acceleration limits $-A_{\max}^{\tau} < A^{\tau} < A_{\max}^{\tau}$, eq. (12) can be rearranged as follows (detailed derivation for eq. (13) is given in Supporting Information):

$$\begin{cases} -\frac{J_{\max}^{\tau}}{(f^*)^2} < \frac{1}{\sigma^3} (m_{uuu}^{\tau} f + 2 m_{uu}^{\tau} f_u + m_u^{\tau} f_{uu}) + \frac{A_{\max}^{\tau}}{\sigma (f^*)^2} f_u \\ < \frac{J_{\max}^{\tau}}{(f^*)^2}, \\ -\frac{J_{\max}^{\tau}}{(f^*)^2} < \frac{1}{\sigma^3} (m_{uuu}^{\tau} f + 2 m_{uu}^{\tau} f_u + m_u^{\tau} f_{uu}) - \frac{A_{\max}^{\tau}}{\sigma (f^*)^2} f_u \\ < \frac{J_{\max}^{\tau}}{(f^*)^2}. \end{cases} \tag{13}$$

Besides, considering the axis velocity of eq. (2) is already linear to the primary feedrate **f**, a new expression of the axis velocity constraint of eq. (4) is given as follows:

$$-\sigma V_{\max}^{\tau} < m_u^{\tau} f < \sigma V_{\max}^{\tau}. \tag{14}$$

3.3 Tangential acceleration linearization

For the linearization of the tangential acceleration $\dot{f}$, one can substitute the tangential acceleration in eq. (3) into eq. (5) to get the following:

$$\left| f_u f / \sigma \right| < A_{c,\max}. \tag{15}$$

Then, similar to the axis acceleration linearization processing, under the preset feedrate upper limit f^*, the tangential acceleration constraint in eq. (15) can be reformulated as follows:

$$-\frac{\sigma A_{c,\max}}{f^*} < f_u < \frac{\sigma A_{c,\max}}{f^*}. \tag{16}$$

3.4 Tangential jerk linearization

For the linearization of the tangential jerk $\ddot{f}$, it is necessary to rewrite the jerk calculation of eq. (3) by combining tangential acceleration term $\dot{f}$ shown as follows:

$$\ddot{f} = (f_{uu} f^2) / \sigma^2 + f_u \dot{f} / \sigma. \tag{17}$$

By substituting eq. (17) into eq. (4), one can get the following:

$$\left| (f_{uu} f^2) / \sigma^2 + f_u \dot{f} / \sigma \right| < J_{c,\max}. \tag{18}$$

By using the similar constraint relaxation operation of eq. (10) to the above formula of eq. (18), one can get an equivalent form shown as follows:

$$\left| (f_{uu} f^2) / (\sigma^2 (f^*)^2) + f_u \dot{f} / (\sigma (f^*)^2) \right| < \frac{J_{c,\max}}{(f^*)^2}. \tag{19}$$

Further, under the given tangential acceleration limit $-A_{c,\max} < \dot{f} < A_{c,\max}$, a new relaxed mathematical expression

of eq. (19) is shown as follows (detailed step by step derivation is shown in Supporting Information):

$$\begin{cases} -\dfrac{J_{c,\max}}{(f^*)^2} < \dfrac{f_{uu}}{\sigma^2} + f_u \dfrac{A_{c,\max}}{\sigma(f^*)^2} < \dfrac{J_{c,\max}}{(f^*)^2}, \\ -\dfrac{J_{c,\max}}{(f^*)^2} < \dfrac{f_{uu}}{\sigma^2} - f_u \dfrac{A_{c,\max}}{\sigma(f^*)^2} < \dfrac{J_{c,\max}}{(f^*)^2}. \end{cases} \tag{20}$$

Substituting eqs. (7) and (8) into eqs. (10), (13), (14), (16) and (20), an explicit linear expression of the constraints with respect to control points $\{D_i\}_0^{Q-1}$ can be derived as shown in eq. (21). Accordingly, the feedrate optimization problem in eq. (6) is now reformulated with relaxed linear constraints and is shown as follows:

Maximize $\int_0^1 \sum_{i=0}^{Q-1} N_{i,k}(u) D_i \mathrm{d}u$,

subject to:

$$\begin{cases} \sum_{i=0}^{Q-1} N_{i,k}(u) D_i < \mathrm{Min.}[f^*, f_{\max}], \\ -\dfrac{\sigma A_{c,\max}}{f^*} < \sum_{i=0}^{Q-1} N'_{i,k}(u) D_i < \dfrac{\sigma A_{c,\max}}{f^*}, \\ \begin{cases} -\dfrac{J_{c,\max}}{(f^*)^2} < \dfrac{1}{\sigma^2}\left(\sum_{i=0}^{Q-1} N''_{i,k}(u) D_i\right) + \dfrac{A_{c,\max}}{\sigma(f^*)^2}\left(\sum_{i=0}^{Q-1} N'_{i,k}(u) D_i\right) < \dfrac{J_{c,\max}}{(f^*)^2}, \\ -\dfrac{J_{c,\max}}{(f^*)^2} < \dfrac{1}{\sigma^2}\left(\sum_{i=0}^{Q-1} N''_{i,k}(u) D_i\right) - \dfrac{A_{c,\max}}{\sigma(f^*)^2}\left(\sum_{i=0}^{Q-1} N'_{i,k}(u) D_i\right) < \dfrac{J_{c,\max}}{(f^*)^2}, \end{cases} \\ -\sigma V^{\tau}_{\max} < m^{\tau}_u \sum_{i=0}^{Q-1} N_{i,k}(u) D_i < \sigma V^{\tau}_{\max}, \\ -\sigma^2 \dfrac{A^{\tau}_{\max}}{f^*} < m^{\tau}_{uu}\left(\sum_{i=0}^{Q-1} N_{i,k}(u) D_i\right) + m^{\tau}_u \left(\sum_{i=0}^{Q-1} N'_{i,k}(u) D_i\right) < \sigma^2 \dfrac{A^{\tau}_{\max}}{f^*}, \\ \begin{cases} -\dfrac{J^{\tau}_{\max}}{(f^*)^2} < \dfrac{1}{\sigma^3}\left(m^{\tau}_{uuu} \sum_{i=0}^{Q-1} N_{i,k}(u) D_i + 2 m^{\tau}_{uu} \sum_{i=0}^{Q-1} N'_{i,k}(u) D_i + m^{\tau}_u \sum_{i=0}^{Q-1} N''_{i,k}(u) D_i\right) + \dfrac{A^{\tau}_{\max}}{\sigma(f^*)^2} \sum_{i=0}^{Q-1} N'_{i,k}(u) D_i < \dfrac{J^{\tau}_{\max}}{(f^*)^2}, \\ -\dfrac{J^{\tau}_{\max}}{(f^*)^2} < \dfrac{1}{\sigma^3}\left(m^{\tau}_{uuu} \sum_{i=0}^{Q-1} N_{i,k}(u) D_i + 2 m^{\tau}_{uu} \sum_{i=0}^{Q-1} N'_{i,k}(u) D_i + m^{\tau}_u \sum_{i=0}^{Q-1} N''_{i,k}(u) D_i\right) - \dfrac{A^{\tau}_{\max}}{\sigma(f^*)^2} \sum_{i=0}^{Q-1} N'_{i,k}(u) D_i < \dfrac{J^{\tau}_{\max}}{(f^*)^2}. \end{cases} \end{cases} \tag{21}$$

In the above eq. (21), how to determine a proper feedrate limit f^* is a key factor for finding the optimal solution. From eq. (1), it is easy to see that the axial dynamics is affected by both the kinematic performance of feed motion and the geometric property of cutter tip curve. Based on the formulation, this means it is very difficult to analytically determine a suitable feedrate for each independent interpolation point under the original constraints of the axis acceleration and the axis jerk limitations. The only exception is that, if the feedrate is kept constant at each parameter position, the near-optimal feedrate limit can be obtained since $\dot{f} = 0$ and $\ddot{f} = 0$. Thus, given arbitrary parameter position u along the toolpath $\mathbf{p}(u)$, an approximate feedrate limit with confined drive constraints can be formulated as follows [14]:

$$f^* = \mathrm{Min.}\left[\frac{\sigma V^{\tau}_{\max}}{|m^{\tau}_u|}, \sqrt{\frac{\sigma^2 A^{\tau}_{\max}}{|m^{\tau}_{uu}|}}, \sqrt[3]{\frac{\sigma^3 J^{\tau}_{\max}}{|m^{\tau}_{uuu}|}}\right]. \tag{22}$$

These formulation and the relax constraints will be used to find the feedrate scheduling profiles and to find the optimal feedrate scheduling for five-axis machining. Details of the optimization algorithm and programmming are presented in the next section.

4 Feedrate optimization with piecewise linear programming scheme

To find the optimal feedrate scheduling, the above mentioned modeling of feedrate optimization problem in eq. (21) is directly used for find feasible feedrate profiles. However, the huge number of cutter location points along the complex five-axis tool path makes real-time solving the feedrate scheduling optimization very challenging, if not impossible. The relaxation method of the nonlinear constraints presented in Sect. 3 makes eq. (21) some easier to be handled. In this section, an algorithm is presented to solve the feed rate scheduling optimization model of eq. (21) in a timely manner. Details are discussed in the following sections.

4.1 Piecewise linear programming scheme

In this paper, an algorithm is presented to solve the feed rate scheduling optimization model in eq. (21) by using a piecewise linear programming scheme with C^2 continuity assurance for adjacent B-spline feed profiles. Figure 3 shows the proposed piecewise linear programming scheme for the feedrate scheduling. Along the given tool-path, its corresponding feed profile is formulated as a set of piecewise B-

spline feed curves rather than a single one [32–36]. As shown in Figure 3, the horizontal coordinate denotes the normalized arc-length parameter of cutter tip path $\mathbf{p}(u)$, and the vertical coordinate indicates the feedrate $\mathbf{f}$. The symbol w_u is used to represent the interval length of path parameter corresponding to each individual B-spline feed curve, and it is usually determined by dividing the path curve with a user defined length or parameter increment. l_u is used to express the overlap range of adjacent feed profiles, which is also called as relaxation distance. In application, l_u can be arbitrarily in the range of $[0.1w_u, 0.3w_u]$, and in this case it can usually maintain the maximum feasible feedrate without compromising machining efficiency. For each predefined parameter interval, the individual feedrate profile is generated, as illustrated in Figure 3. Note that, to achieve a desirable smooth tool motion along the curve path, it is important to ensure the joint between the adjacent B-spline feed curves is at least C^2 continuity so as to avoid any unwanted feedrate fluctuation. What this means is that the adjacent B-spline feed profiles share the same first and second derivatives at the joint points between two adjacent B-spine feed curves. This can be done by carefully choosing the correct control points to satisfy this requirement. Figure 4 shows the feed profile along the predefined parameter range. The feed profile is composed of two parts: the ℓ^{th} B-spline feed curve segment defined in $[u_{\ell,\text{start}}, u_{\ell,\text{end}}]$, and the $(\ell+1)^{\text{th}}$ one defined in $[u_{\ell+1,\text{start}}, u_{\ell+1,\text{end}}]$, as shown in Figure 4. For the convenience of determining each single feed curve segment, both of them will decrease to zero at the end of their own dominated parameter interval, namely $u_{\ell,\text{end}}$ and $u_{\ell+1,\text{end}}$ in Figure 4. A preset relaxation distance l_u, is given to smoothly join two adjacent feed profile. As shown in Figure 4, the initial parameter position of the $(\ell+1)^{\text{th}}$ B-spline feed curve segment, which is also the joint position between the ℓ^{th} and the $(\ell+1)^{\text{th}}$ feed segments, can be calculated by $u_{\ell+1,\text{start}} = u_{\ell,\text{end}} - l_u$. Based on the definition of B-spline feed curve, the ℓ^{th} and $(\ell+1)^{\text{th}}$ feedrate profiles can be expressed as follows.

ℓ^{th} B-spline feed curve:

$$f(t) = \sum_{i=0}^{Q-1} N_{i,k}(t) d_i, t \in [0,1],$$

and

$(\ell+1)^{\text{th}}$ Bspline feed curve:

$$\overline{f}(\overline{t}) = \sum_{i=0}^{\overline{Q}-1} \overline{N}_{i,k}(\overline{t}) \overline{d}_i, \overline{t} \in [0,1],$$

where $N_{i,k}(t)$ (and $\overline{N}_{i,k}(\overline{t})$) represents the B-spline basis function defined based on the knot sequence $T = [t_0, ..., t_{Q+k}]$ (and $\overline{T} = [\overline{t}_0, ..., \overline{t}_{Q+k}]$ for $\overline{N}_{i,k}(\overline{t})$). $\{d_i\}_{i=0}^{Q-1}$ ($\{\overline{d}_i\}_{i=0}^{\overline{Q}-1}$) indicate the control points with the number of $Q(\overline{Q})$. It is worth to mention that, t and $\overline{t}$ are both the normalized parameter with respect to the parameter u, and their corresponding computation formulas are shown as

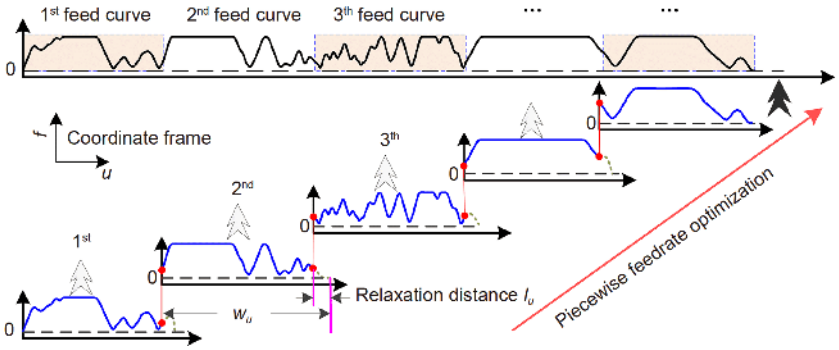

Figure 3 (Color online) Piecewise programming scheme of the B-spline feed profiles.

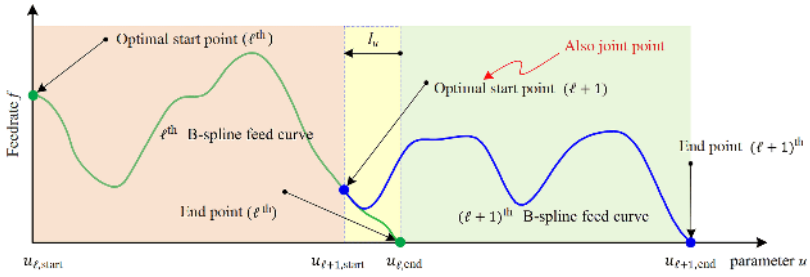

Figure 4 (Color online) Illustration of the C^2 continuous transition between adjacent B-spline feed curves.

$$\begin{cases} t = \dfrac{u-u_{\ell,\text{start}}}{u_{\ell,\text{end}}-u_{\ell,\text{start}}}, \quad u \in [u_{\ell,\text{start}}, u_{\ell,\text{end}}), \\ \bar{t} = \dfrac{u-u_{\ell+1,\text{start}}}{u_{\ell+1,\text{end}}-u_{\ell+1,\text{start}}}, u \in [u_{\ell+1,start}, u_{\ell+1,\text{end}}). \end{cases} \tag{23}$$

When the optimization process of the ℓ^{th} feedrate profile is conducted, the feedrate $f(t(u_{\ell+1,\text{start}}))$ and its associated derivations $f_u(t(u_{\ell+1,\text{start}}))$ and $f_{uu}(t(u_{\ell+1,\text{start}}))$ at the joint parameter position $u_{\ell+1,\text{start}}$ can be obtained by eqs. (7) and (8). To ensure satisfying the C^2 continuity condition, it is required that the $(\ell+1)^{\text{th}}$ feed profile have the same derivations at the joint point. Accordingly, utilizing the Boor-Cox algorithm [37], one can have the equal derivations of $(\ell+1)^{\text{th}}$ B-spline feed curve at the target position $u_{\ell+1,\text{start}}$, where $\bar{t}(u_{\ell+1,\text{start}}) = 0$ by using the mapping function of eq. (23). The condition at the joint point is shown as follows:

$$\begin{cases} \bar{f}(0) = \bar{d}_0, \\ \bar{f}_u(0) = k\dfrac{\bar{d}_1-\bar{d}_0}{\bar{t}_{k+1}-\bar{t}_1}\dfrac{1}{w_{u,\ell+1}}, \\ \bar{f}_{uu}(0) = k(k-1)\dfrac{\dfrac{\bar{d}_2-\bar{d}_1}{\bar{t}_{k+2}-\bar{t}_2}-\dfrac{\bar{d}_1-\bar{d}_0}{\bar{t}_{k+1}-\bar{t}_1}}{\bar{t}_{k+1}-\bar{t}_2}\left(\dfrac{1}{w_{u,\ell+1}}\right)^2, \end{cases} \tag{24}$$

where $w_{u,\ell+1} = u_{\ell+1,\text{end}} - u_{\ell+1,\text{start}}$ is the corresponding parameter range where the $(\ell+1)^{\text{th}}$ B-spline feed curve locates. For satisfying the C^2 continuous condition, it is necessary to let $\bar{f}(0) = f(t(u_{\ell+1,\text{start}})), \bar{f}_u(0) = f_u(t(u_{\ell+1,\text{start}}))$ and $\bar{f}_{uu}(0) = f_{uu}(t(u_{\ell+1,\text{start}}))$. By using eq. (24), the satisfaction condition of C^2 continuity between the ℓ^{th} and $(\ell+1)^{\text{th}}$ feed profiles can be derived as follows:

$$\begin{cases} \bar{d}_0 = f(t(u_{\ell+1,\text{start}})), \\ \bar{d}_1 = \dfrac{f_u(t(u_{\ell+1,\text{start}}))w_{u,\ell+1}(\bar{t}_{k+1}-\bar{t}_1)}{k} \\ \quad +f(t(u_{\ell+1,\text{start}})), \\ \bar{d}_2 = f_{uu}(t(u_{\ell+1,\text{start}}))(w_{u,\ell+1})^2\dfrac{(\bar{t}_{k+1}-\bar{t}_2)(\bar{t}_{k+2}-\bar{t}_2)}{k(k-1)} \\ \quad +\bar{d}_1\dfrac{(-\bar{t}_2+\bar{t}_{k+1}-\bar{t}_1+\bar{t}_{k+2})}{(\bar{t}_{k+1}-\bar{t}_1)}-\bar{d}_0\dfrac{(\bar{t}_{k+2}-\bar{t}_2)}{(\bar{t}_{k+1}-\bar{t}_1)}. \end{cases} \tag{25}$$

For the given 3-degree B-spline feed curve example defined in Sect. 3, let $\bar{t}_0 = \bar{t}_1 = \bar{t}_2 = \bar{t}_3 = 0$. Then, eq. (25) can be further simplified as follows:

$$\begin{cases} \bar{d}_0 = f(t(u_{\ell+1,\text{start}})), \\ \bar{d}_1 = \dfrac{f_u(t(u_{\ell+1,\text{start}}))w_{u,\ell+1}\bar{t}_4}{3}+f(t(u_{\ell+1,\text{start}})), \\ \bar{d}_2 = f_{uu}(t(u_{\ell+1,\text{start}}))(w_{u,\ell+1})^2\dfrac{(\bar{t}_4)(\bar{t}_5)}{6} \\ \quad +\bar{d}_1\dfrac{(\bar{t}_4+\bar{t}_5)}{(\bar{t}_4)}-\bar{d}_0\dfrac{(\bar{t}_5)}{(\bar{t}_4)}. \end{cases} \tag{26}$$

As described before, $f(t(u_{\ell+1,\text{start}}))$, $f_u(t(u_{\ell+1,\text{start}}))$ and $f_{uu}(t(u_{\ell+1,\text{start}}))$ have been calculated in the previous step of finding the ℓ^{th} feedrate scheduling; thus, it is relatively straightforward to obtain the value of $\{\bar{d}_i\}_0^2$ by solving eq. (26). Accordingly, during the next step of finding $(\ell+1)^{\text{th}}$ feedrate scheduling, it only needs to optimize the control points $\{\bar{d}_i\}_3^{\bar{Q}-1}$, while taking the $\{\bar{d}_i\}_0^2$ as the known non-zero boundary condition. The same iterative processing is applied to any adjacently joined two B-spline feed curves for feedrate scheduling.

4.2 Algorithm of solving feedrate scheduling optimization

For modeling the feedrate profile which is composed of the B-spline feedrate curve segments, the knot vector of each individual feed curve segment is selected as follows:

$$U = \left[\underbrace{0,\ldots,0}_{k}, \frac{1}{Q-k}, \ldots, \frac{Q-k-1}{Q-k}, \underbrace{1,\ldots,1}_{k}\right],$$

where Q is the number of control points, and k represents the degree of the B-spline feedrate curve. Based on the derived feedrate optimization model and the introduced piecewise programming scheme presented in the earlier sections, a detailed algorithm to solve the optimization of feedrate scheduling problem is shown as follows.

Inputs: the tool-path information [**p**(u), **o**(u)], the maximum feedrate limit $f_{\max}$, the maximum tangential acceleration $A_{c,\max}$, the maximum tangential jerk $J_{c,\max}$, the maximum axis velocity $V_{\max}^{\tau}$, the maximum axis acceleration $A_{\max}^{\tau}$, the maximum axis jerk $J_{\max}^{\tau}$, the number Γ of B-spline feed curves along the whole tool path curve, the number of sampling points Λ for each segmented tool path, the number Q of control points for each B-spline feed curve, and the relaxation distance l_u.

Output: optimal feed profile in the form of piecewise B-spline curves.

(1) Determine the parameter interval w_u by using the formula:

$$w_u = (1 + l_u(\Gamma-1))/\Gamma.$$

(2) Let p=1.

(3) Set $u_{\text{start}}^p = (p-1)(w_u - l_u)$, and

$$u_{\text{end}}^p = pw_u - (p-1)l_u.$$

(4) For current parameter range of $[u_{\text{start}}^p, u_{\text{end}}^p]$, determine the sampling parameter position $(u_j)_{j=1}^{\Lambda}$ of the path curve, uniformly. And calculate the feedrate upper limit $(f_j^*)_{j=1}^{\Lambda}$ by

using eq. (22).

(5) If p==1, then

optimize the control points $\{d_i^p\}_0^{Q-1}$ for current B-spline feed curve by solving eq. (21).

Else

optimize the control points $\{d_i^p\}_3^{Q-1}$ for current B-spline feed curve by combining eqs. (21) and (26).

End.

(6) p= p+1.

(7) If $p \le \Gamma$, then

go to step (3).

Else

exit the feedrate scheduling module.

End.

The algorithm is used to solve the optimization of feed rate scheduling problem for five-axis machining. In the next section, computer implementation and the laboratory experiments for validation are presented.

5 Computer simulation and laboratory experiments for verification

In this section, both the computer simulations and the laboratory experiments of feedrate scheduling are presented. Several different examples with the NURBS tool paths are used in the experiments to validate the proposed feedrate scheduling method. Actual machining of example parts were conducted on multi-axis machine tools at our manufacturing research lab.

As shown in Figure 5, a tilting-rotary-table five-axis machine tool with an open architecture controller is used in the validation experiment tests, which allows the direct implementation of the developed feedrate scheduling algorithm into the CNC controller system. The feed motion of each axis is driven by the YASKAWA servo motors and axis drivers. The position feedback signals of the translational axes and rotational axes are fed back directly from linear optical encoders with a resolution of 500 × 256 pulses/rev, and the actual velocity of each axis can be obtained by differentiating

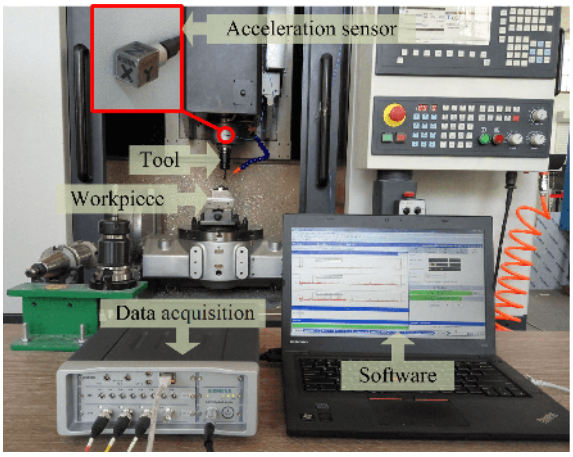

Figure 5 (Color online) Five-axis machine test bed.

the positions with respect to the unit time and high-frequency noise is removed with a low-pass filter in the implemented CNC open architecture controller system. Three different examples were used for experiments. Details of the experiments are presented in the following sections.

5.1 Comparative simulations

Figure 6(a) shows the first example of a complex wild goose-shape like tool-path, which is expressed by a B-spline curve with 251 control points and a length of 246.951 mm. In this feedrate scheduling testing example, 80 control points were used to model the target B-spline feedrate curve, and 500 evaluation points were sampled along the tool-path by a preset parameter interval. Detailed comparisons were first performed between the proposed method and the discrete numerical (DN) method and the recent linear programming (LP) method [35]. All the algorithms were coded by using Matlab software and ran on an Intel Core i7-4790k 4.0 GHz personal computer with Windows7 operating system. As stated earlier, the machining process related constraints are often designed by the requirement of process planner or the machines itself, and the magnitudes of the corresponding constraints used in the feedrate scheduling testing are selected from one of the general cases [32–35], for example,

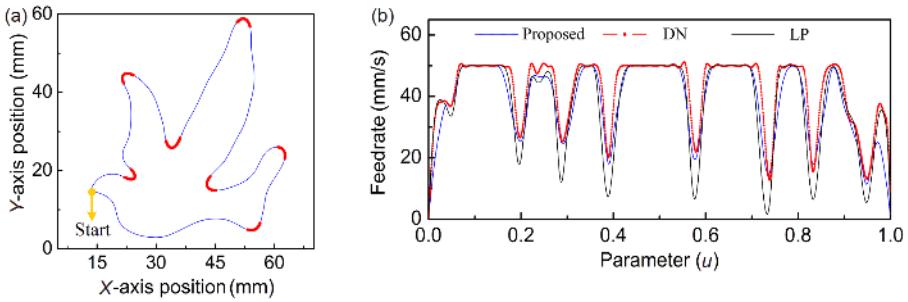

Figure 6 (Color online) (a) Simulation results for the wild goose curve tool path; (b) optimal feedrate profiles using different optimization methods.

$\mathbf{J}_{max} = (10 \sim 30)\mathbf{A}_{max}$ and $\mathbf{A}_{max} = (5 \sim 15)\mathbf{V}_{max}$, as shown in Table 1. Notice that, in this testing, all these three algorithms were run on a single B-spline tool-path, so that the effect of other factors, such as moving windows or parallel windows, were not considered in this experiment.

Figure 6(b) shows the optimal feedrate curves by using three different methods. In Figure 6(b), it can be seen that, in the result generated by the DN method, there are some undesirable fluctuations at the high-speed transition zones on the feedrate profile, and this phenomenon is mainly caused by the subsequent curve fitting to the sampling points. By contrast, the results generated by the proposed method and the LP method show better smooth performance as shown in Figure 6(b).

For comparison, Table 2 shows the computation time of the three methods and the machining time obtained according to the three different generated feedrate curves. From Table 2, it can be seen that the running time and the machining time by the DN method is less than that of the other two methods. The running time of the proposed method is nearly identical to that of the LP method, while the proposed method has a reduction of 18.137% in machining time over the LP method. Figure 7 shows the results of axis velocity, axis acceleration, and axis jerks generated by these three methods. As shown in Figure 7, both the proposed method and the LP method can comply with the axis acceleration and the axis jerk limits within the allowable ranges [–300 mm/s^2, 300 mm/s^2] and [–6000 mm/s^3, 6000 mm/s^3], although a tiny constraint variations exist by using LP methods. In addition, it also needs to mention that the machining efficiency of LP method can be further improved with the increase of the number of control points of the feedrate curve, but to some extent, the tendency and magnitude of constraint violations become more obvious when using LP method. By contrast, the proposed method has a better controllability in limiting axis accelerations and jerks, even though a larger number of control points of feedrate curve are specified. From Figure 7 it also shows that the results generated by the DN method violate the capacity limits with a maximum axis acceleration of 380.434 mm/s^2 and a maximum axis jerk of 9473.361 mm/s^3, exceeding both the maximum allowed capacity limits. Overall, the proposed method indicates a reliable performance of constraint limits in the example as

Table 1 Constraints in feedrate scheduling

Parameter	Limit value	Unit
Maximum feedrate	50	mm/s
Sampling period	4	ms
Linear axis velocity	50	mm/s
Linear axis acceleration	300	mm/s^2
Linear axis jerk	6000	mm/s^3

Table 2 Comparison of different feedrate scheduling methods

Optimization method	Execution time (s)	Machining time (s)	Machining time reduction
DN	7.908	6.764	–31.232%
LP	13.274	9.836	–
Proposed	13.888	8.052	–18.137%

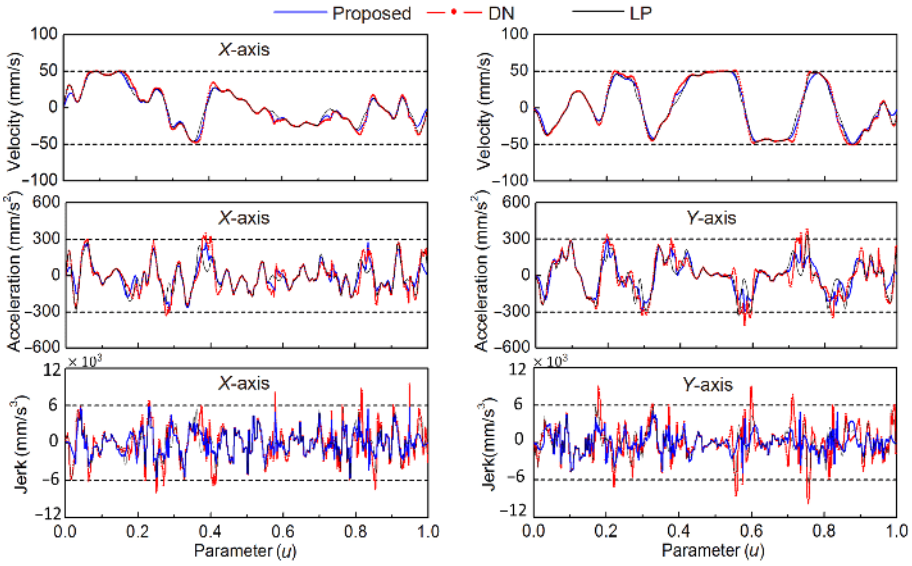

Figure 7 (Color online) Comparison of the driving performance of the proposed method, DN and LP.

shown in Table 2 and Figure 7.

5.2 Flank milling experiment

Figure 8(a) shows the second example of the free-form surface machining with five-axis tool motions by a flank milling. In this five-axis machining example, it has a total tool path length of 114.488 mm and the five-axis tool path is expressed by dual NURBS curves with a total of 400 control points. For computing the feedrate, the number of B-spline feed curve segments along the entire tool-path is set as 2, and the number of control points of each B-spline feed curve segment is given as 150. Figure 8(b) shows the final optimal feedrate profile generated by the proposed feedrate scheduling algorithm. In Figure 8(b), it can be seen there exist several slowdown areas along the tool path trajectory in accordance with the limits of the axis velocity, the axis acceleration and the axis jerk. The proposed algorithm generated axis velocities of both the translation axes and the rotational axes are shown in Figure 8(c)–(d). The results in Figure 8(c)–(d) show the axis velocities generated by the proposed method performs within the maximum allowable ranges of [–30 mm/s, 30 mm/s] and [–0.3 rad/s, 0.3 rad/s]. Figure 8(e)–(h) shows the proposed algorithm generated axis accelerations and axis jerks of all five involved drive axes. Although some slight deviation occurs due to the high frequency noise and signals in the electric drive system, they all successfully perform within the acceptable machine capacity limit ranges of [–100 mm/s^2, 100 mm/s^2], [–1 rad/s^2, 1 rad/s^2], [–1000 mm/s^3, 1000 mm/s^3] and [–10 rad/s^2, 10 rad/s^2], as shown in Figure 8(e)–(h). The example shown in Figure 8 demonstrates the proposed method can successfully generate an optimal feed rate scheduling subject to the machine tool driving axis capacity limits for five-axis machining without the unfavorable violation of machine capacity limits that other methods suffered.

5.3 Experiment on end milling machining

Figure 9 shows the third experiment of machining a sculptured surface part. As shown in Figure 9, the tool path on curved surfaces is represented as NURBS path with 600 control points and the tool path has a path length of 708.928 mm on the example part surface. The constraints used in the third feedrate scheduling experiment are summarized in Table 3. The number of B-spline feed curves segments along the tool path curve is set as 10, and there are 3000 data points sampled for constraint evaluation along the path curve segment. The maximum programmed feedrate limit in machining is preset as 15 mm/s.

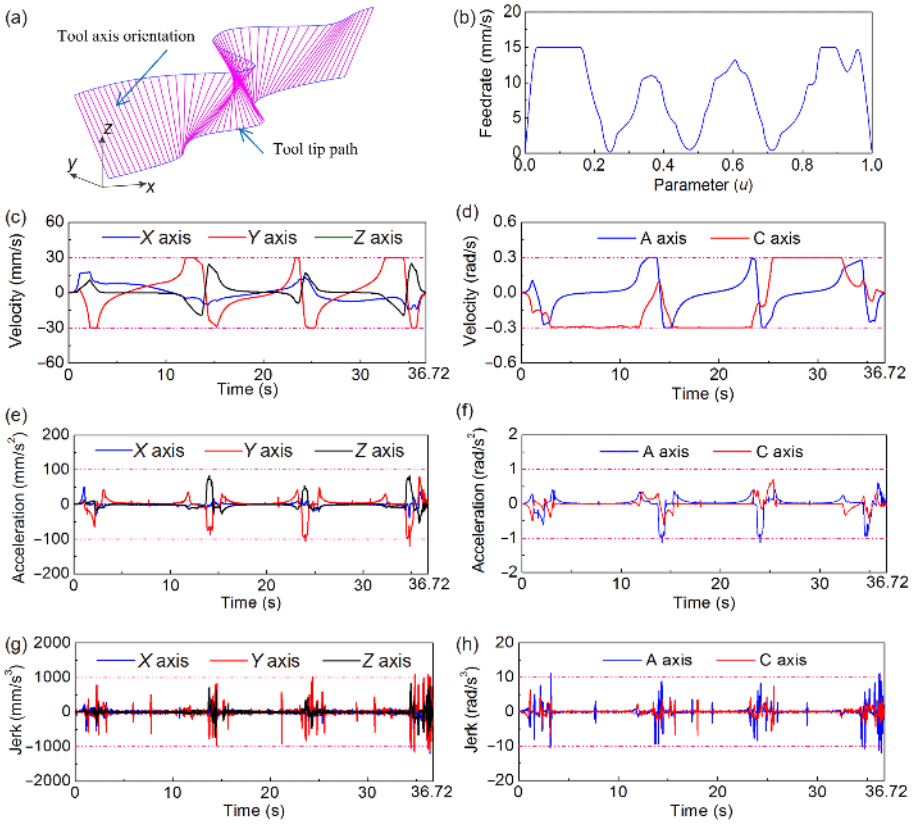

Figure 8 (Color online) Experimental results. (a) Too path; (b) feedrate profile; (c) axis velocities of translational axes; (d) axis velocities of rotary axes; (e) axis accelerations of translational axes; (f) axis accelerations of rotary axes; (g) axis jerks of translational axes; (h) axis jerks of rotary axes.

Using the proposed computation method and the optimization algorithm, the generated feedrate profile is shown in Figure 10(a). Figure 10(b)–(d) shows the corresponding axis velocity, the axis acceleration and the axis jerk of each individual drive axis movement. From the results shown in Figure 10, one can see that the axis performances of all involved axes have been successfully confined within their maximum allowable ranges.

For the validation purpose, Figure 11 shows a physical machining experiment conducted on an example part of aluminum alloy AL Alloy 6061 machined with a 10 mm diameter ball-end carbide cutter. In this practical implementation, the machine vibration intensity generated by the proposed jerk-limited interpolation method are measured and compared with the case of constant-speed machining (15 mm/s). In the machining experiment, the measurement

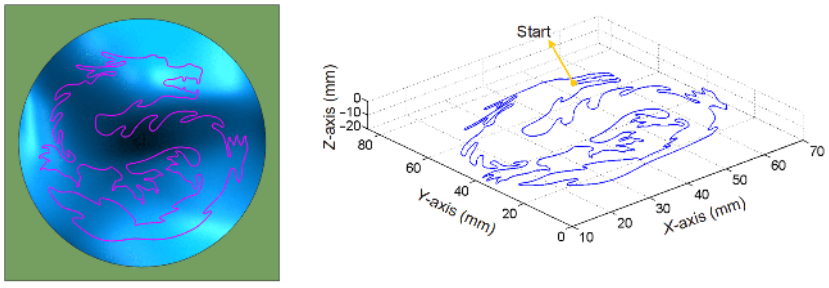

Figure 9 (Color online) Three-axis long path used for the end milling.

Table 3 Constraints in feedrate scheduling for experiments

Parameter	Flank milling	End milling	Unit
Maximum feedrate	15	15	mm/s
Sampling period	4	4	ms
Linear axis velocity	30	–	mm/s
Rotary axis velocity	0.3	–	rad/s
Linear axis acceleration	100	100	mm/s^2
Rotary axis acceleration	1	–	rad/s^2
Linear axis jerk	1000	1000	mm/s^3
Rotary axis jerk	10	–	rad/s^3

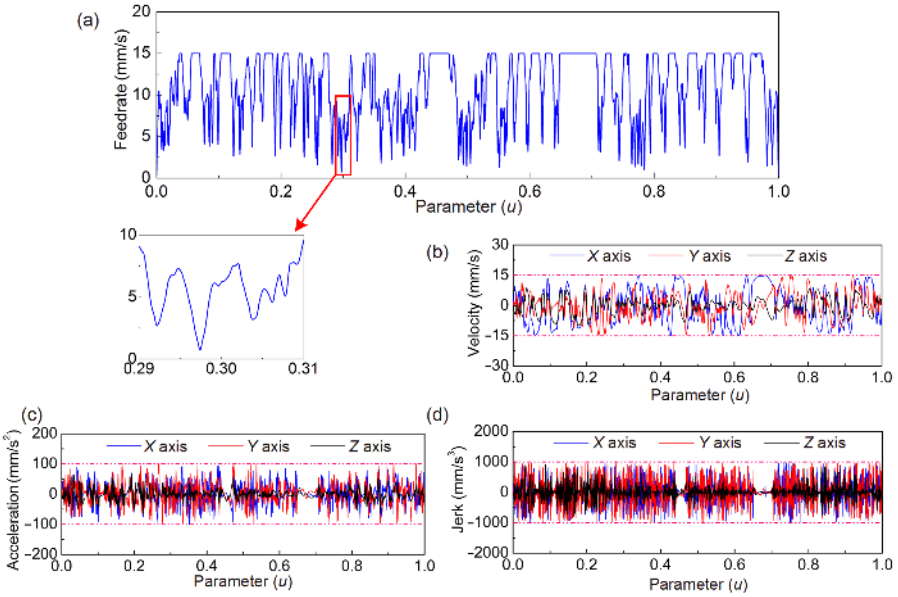

Figure 10 (Color online) Feedrate scheduling results. (a) Optimal feedrate profile; (b) axis velocity of each drive; (c) axis acceleration of each drive; (d) axis jerk of each drive.

devices used is a fast signal acquisition and analysis system LMS SCADAS3, as shown earlier in Figure 5. Figure 11 shows two final machined parts: one without the jerk constraint in feed rate scheduling, and the second one with the proposed jerk constraint in optimizing feedrate scheduling. From Figure 11, one can see that the jerk-limited feedrate scheduling optimization method exhibits a satisfactory performance and a better surface finish compar-ing to the one with only the traditional constant-speed case. As shown in Figure 11, the machined part example demonstrates a good machining consistency and no obvious vibration or jerk even at the problematic highly curved tool trajectory.

Figure 12 shows the detailed axial performance with the measured vibration frequency spectrum diagrams for the two different cases. Based on the actual data measured in the experiment shown in Figure 12, the experimental results show that the vibration of the machine tool by the traditional constant-speed machining case is rather wildly fluctuating, especially at the frequency of near 300, 500 and 600 Hz. On the other hand, in Figure 12, the proposed jerk-limited optimization method performs much better in reducing the mechanical vibrations and jerks in machining. In Figure 12, one can find the result generated by the proposed method shows the vibrations at those critical frequencies has been fully under controlled. The presented experiment results demonstrate that the presented computation method and the proposed optimization algorithm are capable to achieve good dynamic performances of the machine tool that leads into the improvement of the machining accuracy and machined surface quality.

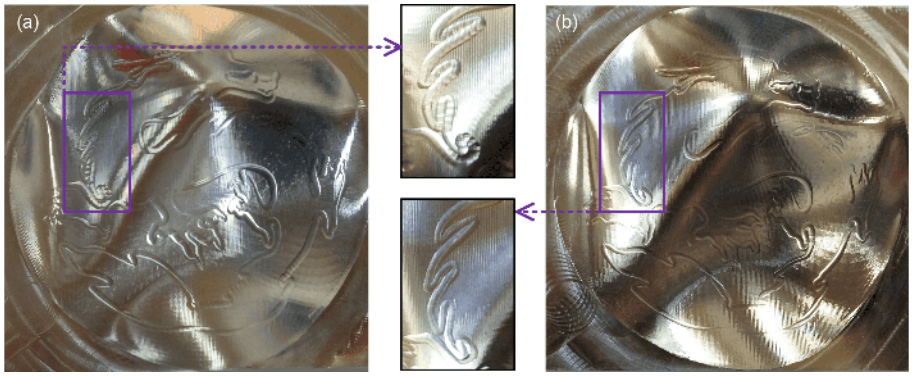

Figure 11 (Color online) Comparison of physical cutting results for different scheduled feedrate profiles. (a) Machined part without jerk constraint; (b) machined part with jerk constraint.

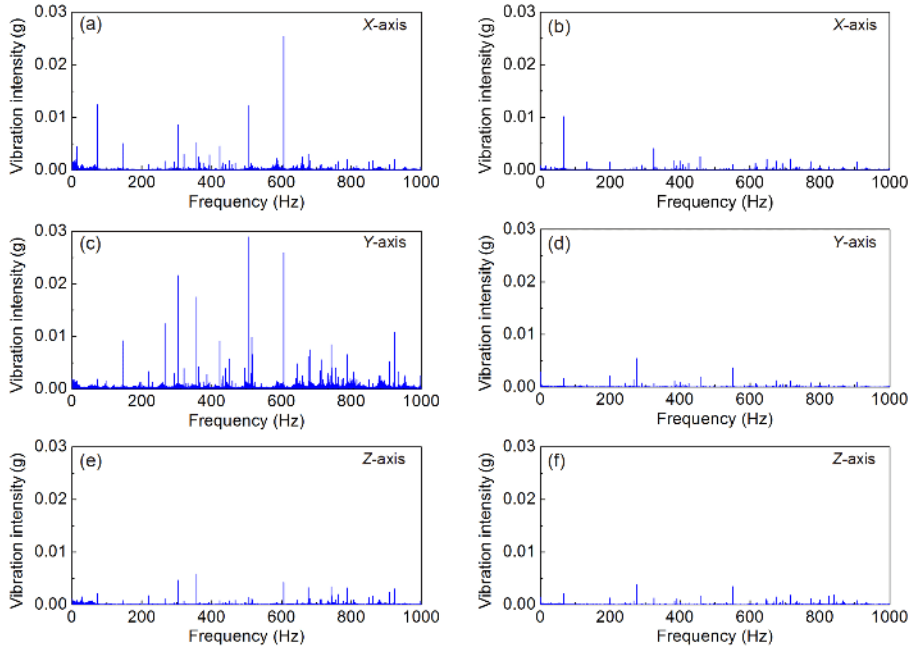

Figure 12 (Color online) Comparison of the vibration on servo drives for different scheduled feedrate profiles. (a) *X*-axis vibration without jerk constraints; (b) *X*-axis vibration with jerk constraints; (c) *Y*-axis vibration without jerk constraints; (d) *Y*-axis vibration with jerk constraints; (e) *Z*-axis vibration without jerk constraints; (f) *Z*-axis vibration with jerk constraints.

6 Conclusions

In this paper, a new computation method and an optimization algorithm have been presented for feedrate scheduling of five-axis machining with constraints of both the machine axis jerk limit and the process limit. The presented method first relaxes the nonlinear constraints of the machine servo drive and the cutter tip movement limits. An explicit analytical solution to the optimal feedrate profile, which is expressed by B-splines, can be obtained with compliance of machine tool feasibility and machine axis capacity limits. The presented method provides a way that all of the machining-related constraints, in terms of the machines' axis velocities, accelerations and jerks as well as the process constraints of cutter tip, are capable of being analytically linearized by the primary variable of feedrate. A piecewise optimization scheme is introduced with the C^2 continuity assurance between adjacent feedrate profiles for optimization. An optimization algorithm is then presented to find the optimal feedrate scheduling for five-axis machining. Experiments on both the computer implementation and the laboratory actual machining of practical parts were conducted for verification. Compared with the existing numerical methods, the presented method provides an accurate analytical solution to the constrained feedrate scheduling without compromising the machining efficiency. And it also exhibits a strong controllability in limiting axis accelerations and jerks. The presented technique can be used for computer aided manufacturing and the CNC machine tool controller systems applications. However, its computing cost and machining efficiency still need further validation for real application.

This work was supported by the National Natural Science Foundation of China (Grant No. 51525501), the Science Challenge Project (Grant No. TZ2016006-0102), and the Dalian Science and Technology Project (Grant No. 2016RD08). Dr. Y.S. Lee was partially supported by the National Science Foundation (Grant No. CMMI-1547105) to North Carolina State University.

Supporting Information

The supporting information is available online at tech.scichina.com and link.springer.com. The supporting materials are published as submitted, without typesetting or editing. The responsibility for scientific accuracy and content remains entirely with the authors.

1 Lo C C. Real-time generation and control of cutter path for 5-axis CNC machining. Int J Machine Tools Manufacture, 1997, 39: 471–488
2 Langeron J M, Duc E, Lartigue C, et al. A new format for 5-axis tool path computation, using bspline curves. Comput-Aided Des, 2004, 36: 1219–1229
3 Chen D, Dong L, Bian Y, et al. Prediction and identification of rotary axes error of non-orthogonal five-axis machine tool. Int J Machine Tools Manufacture, 2005, 94: 74–87
4 Bi Q, Huang N, Sun C, et al. Identification and compensation of geometric errors of rotary axes on five-axis machine by on-machine measurement. Int J Machine Tools Manufacture, 2015, 89: 182–191
5 Lee J H, Liu Y, Yang S H. Accuracy improvement of miniaturized machine tool: Geometric error modeling and compensation. Int J Machine Tools Manufacture, 2006, 46: 1508–1516
6 Sun Y, Sun S, Xu J, et al. A unified method of generating tool path based on multiple vector fields for CNC machining of compound NURBS surfaces. Comput-Aided Des, 2017, 91: 14–26
7 Gong H, Wang Y, Song L, et al. Spiral tool path generation for diamond turning optical freeform surfaces of quasi-revolution. Comput-Aided Des, 2015, 59: 15–22
8 Li X F, Zhao H, Zhao X, et al. Interpolation-based contour error estimation and component-based contouring control for five-axis CNC machine tools. Sci China Tech Sci, 2018, 61: 1666–1678
9 Sencer B, Altintas Y. Modeling and control of contouring errors for five-axis machine tools—Part II: Precision contour controller design. J Manuf Sci Eng, 2009, 131: 031007
10 Mansour S Z, Seethaler R. Feedrate optimization for computer numerically controlled machine tools using modeled and measured process constraints. J Manuf Sci Eng, 2017, 139: 011012
11 Chen M, Sun Y. A moving knot sequence-based feedrate scheduling method of parametric interpolator for CNC machining with contour error and drive constraints. Int J Adv Manuf Technol, 2018, 98: 487–504
12 Rahaman M, Seethaler R, Yellowley I. A new approach to contour error control in high speed machining. Int J Machine Tools Manufacture, 2015, 88: 42–50
13 Qiao Z, Wang T, Wang Y, et al. Bézier polygons for the linearization of dual NURBS curve in five-axis sculptured surface machining. Int J Machine Tools Manufacture, 2013, 53: 107–117
14 Beudaert X, Pechard P Y, Tournier C. 5-axis tool path smoothing based on drive constraints. Int J Machine Tools Manufacture, 2011, 51: 958–965
15 Yang J, Altintas Y. Generalized kinematics of five-axis serial machines with non-singular tool path generation. Int J Machine Tools Manufacture, 2013, 75: 119–132
16 Yuen A, Zhang K, Altintas Y. Smooth trajectory generation for five-axis machine tools. Int J Machine Tools Manufacture, 2013, 71: 11–19
17 Huang J, Du X, Zhu L M. Real-time local smoothing for five-axis linear toolpath considering smoothing error constraints. Int J Machine Tools Manufacture, 2018, 124: 67–79
18 Yong T, Narayanaswami R. A parametric interpolator with confined chord errors, acceleration and deceleration for NC machining. Comput-Aided Des, 2003, 35: 1249–1259
19 Erdim H, Lazoglu I, Ozturk B. Feedrate scheduling strategies for free-form surfaces. Int J Machine Tools Manufacture, 2006, 46: 747–757
20 Kim S J, Lee H U, Cho D W. Feedrate scheduling for indexable end milling process based on an improved cutting force model. Int J Machine Tools Manufacture, 2006, 46: 1589–1597
21 Erkorkmaz K, Altintas Y. Quintic spline interpolation with minimal feed fluctuation. J Manuf Sci Eng, 2005, 127: 339–349
22 Jin Y, He Y, Fu J, et al. A fine-interpolation-based parametric interpolation method with a novel real-time look-ahead algorithm. Comput-Aided Des, 2014, 55: 37–48
23 Liu X, Ahmad F, Yamazaki K, et al. Adaptive interpolation scheme for NURBS curves with the integration of machining dynamics. Int J Machine Tools Manufacture, 2005, 45: 433–444
24 Wang Y, Yang D, Gai R, et al. Design of trigonometric velocity scheduling algorithm based on pre-interpolation and look-ahead interpolation. Int J Machine Tools Manufacture, 2015, 96: 94–105
25 Annoni M, Bardine A, Campanelli S, et al. A real-time configurable NURBS interpolator with bounded acceleration, jerk and chord error. Comput-Aided Des, 2012, 44: 509–521
26 Lin M T, Tsai M S, Yau H T. Development of a dynamics-based NURBS interpolator with real-time look-ahead algorithm. Int J Machine Tools Manufacture, 2007, 47: 2246–2262
27 Beudaert X, Lavernhe S, Tournier C. Feedrate interpolation with axis jerk constraints on 5-axis NURBS and G1 tool path. Int J Machine Tools Manufacture, 2012, 57: 73–82

28 Dong J, Ferreira P M, Stori J A. Feed-rate optimization with jerk constraints for generating minimum-time trajectories. Int J Machine Tools Manufacture, 2007, 47: 1941–1955
29 Sun Y, Zhao Y, Bao Y, et al. A smooth curve evolution approach to the feedrate planning on five-axis toolpath with geometric and kinematic constraints. Int J Machine Tools Manufacture, 2015, 97: 86–97
30 Sencer B, Altintas Y, Croft E. Feed optimization for five-axis CNC machine tools with drive constraints. Int J Machine Tools Manufacture, 2008, 48: 733–745
31 Zhang K, Yuan C M, Gao X S, et al. A greedy algorithm for feedrate planning of CNC machines along curved tool paths with confined jerk. Robotics Comput-Integrated Manufacturing, 2012, 28: 472–483
32 Fan W, Gao X S, Lee C H, et al. Time-optimal interpolation for five-axis CNC machining along parametric tool path based on linear programming. Int J Adv Manuf Technol, 2013, 69: 1373–1388
33 Guo J X, Zhang K, Zhang Q, et al. Efficient time-optimal feedrate planning under dynamic constraints for a high-order CNC servo system. Comput-Aided Des, 2013, 45: 1538–1546
34 Liu H, Liu Q, Sun P, et al. The optimal feedrate planning on five-axis parametric tool path with geometric and kinematic constraints for CNC machine tools. Int J Production Res, 2017, 55: 3715–3731
35 Erkorkmaz K, Chen Q G C, Zhao M Y, et al. Linear programming and windowing based feedrate optimization for spline toolpaths. CIRP Ann, 2017, 66: 393–396
36 Zhou J, Sun Y, Guo D. Adaptive feedrate interpolation with multi-constraints for five-axis parametric toolpath. Int J Adv Manuf Technol, 2014, 71: 1873–1882
37 Pigel L, Tiller W. The NURBS Book. 2nd ed. Berlin: Springer, 1997